Available online at www.sciencedirect.com
ScienceDirect
Trans. Nonferrous Met. Soc. China 30(2020) 1135−1147
Transactions of Nonferrous Metals Society of China
www.tnmsc.cn

# Effect of Cu addition on microstructural evolution and hardening of mechanically alloyed Al−Ti−O in-situ composite

A. S. PROSVIRYAKOV, A. I. BAZLOV, I. S. LOGINOVA

Department of Physical Metallurgy of Non-Ferrous Metals,
National University of Science and Technology "MISiS", Leninskiy Prospect 4, Moscow 119049, Russia

Received 23 August 2019; accepted 17 February 2020

**Abstract:** The microstructure formation and strengthening of an Al−5wt.%$TiO_2$ composites with additions of 5 wt.% Cu and 2 wt.% stearic acid (as a process control agent, PCA) during mechanical alloying and subsequent thermal exposure were studied. The powder composites were prepared by high-energy ball milling for up to 10 h. Single line tracks of the powders were laser melted. Optical and scanning electron microscopy, XRD analysis and differential scanning calorimetry were used to study microstructural evolution. The results showed that the Cu addition promotes an effective mechanical alloying of aluminum with $TiO_2$ from the start of milling, resulting in higher microhardness (up to HV 290), while the PCA, on the contrary, postpones this process. In both cases, the composite granules with uniform distribution of $TiO_2$ particles were formed. Subsequent heating of mechanically alloyed materials causes the activation of an exothermic reaction of $TiO_2$ reduction with aluminum, the start temperature of which, in the case of Cu addition, shifts to lower values, that is, the transformation begins in the solid state. Besides, the Cu-added material after laser melting demonstrates a more dispersed and uniform structure which positively affects its microhardness.
**Key words:** mechanical alloying; Al−Ti−O system; aluminum matrix composites; microstructure; hardening; laser melting

## 1 Introduction

Additive manufacturing is a modern and rapidly growing industry, gaining popularity around the world. This is due to the fact that this type of production allows to produce parts without any special tools and shortens the production cycle, providing significant savings in time and resources [1]. Technologies such as selective laser melting (SLM) and direct laser deposition (DLD) are increasingly used for the production of critical parts of complex shape from aluminum alloys for use in the automotive and aerospace industry. In a SLM technique, a uniform "bed" of metal powder is first deposited and then specific regions of the "bed" are melted by the laser beam in order to build a single layer of the part. Instead of forming a layer of material and selective energy delivery process, DLD combines the powder/energy delivery for simultaneous deposition and part forming within a similar region [2].

However, aluminum alloys used in additive manufacturing are limited mainly by the Al−Si system [1,3−5]. In this regard, currently, studies are underway to expand the range of alloys that are suitable for this type of production, with improved strength properties. Thus, increased focus is on the Al−Cu system, which demonstrates good results [6−8]. In order to significantly improve the strength properties of aluminum alloys subjected to laser melting, recently attempts have been made to use the aluminum matrix composites (AMC) strengthened by various ceramic particles as the materials for the additive manufacturing [4,5,9,10]. At the same time, the creation of "in situ" composite

**Corresponding author:** A. S. PROSVIRYAKOV; E-mail: pro.alex@mail.ru
DOI: 10.1016/S1003-6326(20)65284-0

materials in which hardening particles are formed as a result of laser irradiation, for example, in the Ti−Al−C system [11], looks promising. In such composite materials, the interphase boundaries are free from contamination, which provides a good connection between the matrix and particles and, as a result, a more efficient load transfer across the interphase boundary, which results in higher mechanical characteristics compared to composites made using traditional methods [12,13].

Among systems in which hardening particles can be synthesized in situ directly in a metal matrix, the Al−Ti−O system is of particular interest. In this system, the synthesis of refractory particles of titanium aluminide and alumina occurs as a result of an aluminothermic reaction initiated by heating a mechanically alloyed Al−$TiO_2$ powder mixture [14−26]. Mechanical alloying [27,28] allows to achieve a homogeneous fine structure and uniform distribution of particles of alloying components. The features of the aluminothermic reaction, as well as the final structure of materials containing the maximum fraction of reaction products (aluminum oxide and titanium aluminide), are well studied. The previously obtained results demonstrate good prospects for achieving high strength properties due to the effect of dispersion hardening by synthesized particles. However, the structure formation of low-alloyed AMC containing in the initial state less than 10 wt.% $TiO_2$ has not been practically studied. In addition, the influence of alloying elements, for example, copper, in the process of forming the structure of in situ strengthened materials is not known. As already noted, the Al−Cu system is a suitable basis for creating new materials with increased strength for use in additive manufacturing.

Thus, the aim of this work is to study the effect of copper addition on the structure formation and strengthening of an Al−Ti−O composite with a low $TiO_2$ content during mechanical alloying and subsequent thermal exposure.

## 2 Experimental

As the main starting materials, aluminum powders with a purity of not less than 99.0% with a particle size of about 450 μm and titanium oxide of technical purity (not less than 92.0%) with a particle size of about 1 μm were used. The content of rutile titanium oxide in the initial powder mixtures was 5 wt.%. In this work, materials of two different compositions were investigated. In the first case, copper was used as an alloying element (purity not less than 99.5%) in the form of a powder with a particle size of not more than 100 μm in an amount of 5 wt.%. In the second case, stearic acid was added as a process control agent (PCA) in an amount of 2 wt.%. Such content is effective to prevent excessive weldability of the powder material in the process of high-energy milling and to achieve a small particle size [29]. The powder mixtures were processed on a Retsch PM400 planetary ball mill in an argon atmosphere. The ball-to-powder mass ratio (BPR) and the milling speed were 20:1 and 300 r/min, respectively.

To study the morphology and microhardness of the powders, special samples were prepared using acrylic cold-mounting plastic in a ratio of 1:1. The morphology of the powder particles was examined with an Axiovert 200 MAT optical microscope. The microhardness was measured by the Vickers method on a Wolpert & Wilson 402MVD tester at a load of 25−50 g. X-ray diffraction (XRD) analysis was performed on a D8 Discover diffractometer (Bruker-AXS) with Cu $K_\alpha$ radiation. The initial processing of X-ray lines and the calculation of the integral width and center of gravity were carried out using the OUTSET program [30]. The microstructure was examined using a TESCAN VEGA 3LMH scanning electron microscope (SEM) equipped with an XMAX−80 energy dispersive (EDS) analyzer, in the mode of backscattered electrons. Differential scanning calorimetry (DSC) was performed using a Setaram Labsys 1600 calorimeter with a heating rate of 20 K/min in an argon atmosphere.

Laser melting of the powders was performed on an aluminum substrate on a MUL−1−M−200 device equipped with a Nd:YAG laser with a radiation wavelength of 1064 nm. The focal length was 100 mm, the scanning speed was 1 mm/s, the pulse duration was 14 ms, and the frequency was 5 Hz. The diameter of the laser spot varied from 0.5 to 1.5 mm. Argon of high purity was used as a shielding gas, supplied to the treatment zone under a pressure of 0.6 MPa using a cylindrical nozzle.

## 3 Results and discussion

### 3.1 Microstructural evolution during mechanical alloying

The formation of granules of metal-matrix composites during mechanical alloying occurs as a result of repeated alternations of the processes of deformation, welding and fracture of metal particles under the shock-abrasive effect of the grinding balls [31]. In order to trace the process of mechanical alloying of aluminum with titanium oxide particles and the influence of copper and PCA additives on it, we studied the morphology of the material particles during high-energy processing in a planetary mill. It should be noted that, as preliminary studies have shown, the processing of pure aluminum with 5 wt.% titanium oxide without any additions according to the mode used is impossible due to the excessive weldability of aluminum particles. Since aluminum is very ductile, particles, as a result of intense plastic deformation accompanying the milling process, are welded together and onto grinding balls until they are completely covered with a uniform layer. At the same time, the destruction of this aluminum shell covering the steel balls does not occur with an increase in the processing time, which makes the mechanical alloying process impossible.

Images of powder particles of Al−5$TiO_2$ with 5 wt.% Cu and 2 wt.% stearic acid obtained using optical microscopy are presented in Fig. 1. Figure 1(a) shows that after 1 h of treatment, in the case of using a PCA, the particle size of aluminum, in comparison with the original, remains virtually unchanged. As a result of the influence of the grinding balls, the particles are deformed, acquiring an irregular shape. A subsequent increase in the

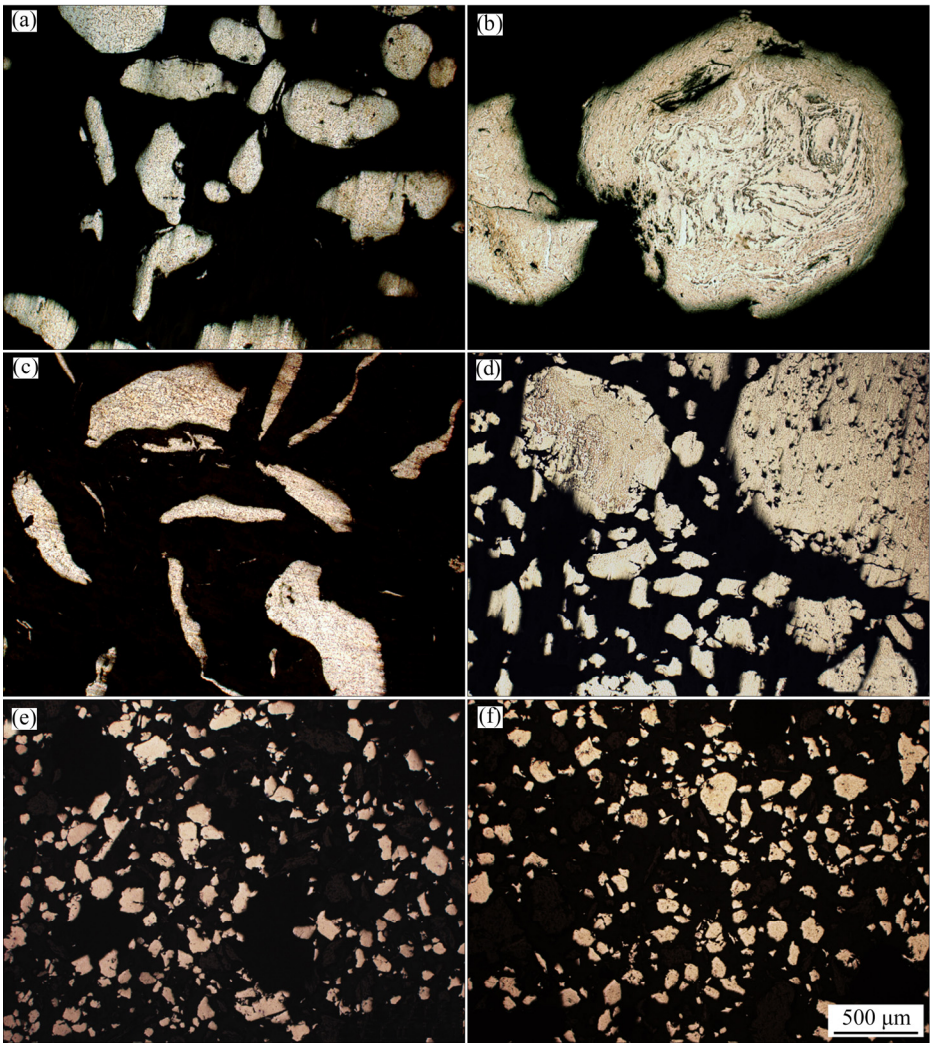


**Fig. 1** Optical microscopy images of powder particles of Al−5$TiO_2$ with 2 wt.% PCA after 1 h (a), 6 h (c) and 10 h (e) of milling, and also with 5 wt.% Cu after 1 h (b), 6 h (d) and 10 h (f)

processing time leads to even greater change. So, as a result of intense plastic deformation after 3 h, the shape of aluminum particles becomes more elongated and flattened, continuing to remain so even after 8 h of treatment. An example of such a morphology observed in the range of 3−8 h is given in Fig. 1(c), which was obtained for the particles milled for 6 h. Thus, the presence of PCA in the material leads to the suppression of particle welding, and is necessary for the formation of granules of the composite material. This is due to the fact that surfactant is adsorbed on the surface of aluminum particles, reducing surface tension, which leads to the appearance of a lubricating effect [27]. However, after 10 h, the particles acquired a relatively regular shape (Fig. 1(e)), while their average size decreased to 63 μm.

A completely different image is observed in the case of a change in the morphology of Al−5$TiO_2$ particles with the copper addition. So, after 1 h of processing (Fig. 1(b)), we see rather large particles with a size of about 1000 μm, which have a characteristic layered structure that occurs during high-energy milling of two ductile metals, aluminum and zirconium [32]. In this case, such composite granules were formed as a result of multiple processes of cold welding of aluminum and copper particles, which were welded onto each other. On the microstructure, areas of pure aluminum and areas (inclusions) of copper are visible. With an increase in the duration of mechanical alloying, the degree of plastic deformation and hardening of welded particles increases, which causes their subsequent fracture. The alternation of processes of plastic deformation and cold welding is an indispensable condition for the occurrence of mechanical alloying. So, in Fig. 1(d), after 6 h of treatment, both large undestroyed particles and smaller ones are visible. Moreover, if the structure of large granules continues to remain heterogeneous due to the alternation of regions of different chemical compositions, then the structure of the crushed particles is homogeneous. A further increase in time up to 10 h leads to the fact that the processed material consists entirely of milled and homogeneous particles of relatively regular shape, and the average size is about 60 μm (Fig. 1(f)).

Particles of titanium oxide in the granules microstructure of the investigated materials are not detectable by optical microscopy. To detect them, scanning electron microscopy was used, and the results are presented in Fig. 2. In the images of the powder granules of both materials, after 10 h of treatment, light particles of titanium oxide are uniformly distributed in a dark aluminum matrix. The identification of light particles was carried out using energy dispersive analysis. So, Fig. 3 shows the distribution of elements in Al−5$TiO_2$−5Cu. A comparison of images of various regions of the granules obtained in backscattered electrons with images obtained in the characteristic radiation of Al, Ti, O, and Cu confirms that the visible particles are titanium oxide. Thus, both materials at the end of mechanical alloying consist of two phases: Al and $TiO_2$. The absence of traces of copper in the Al−5$TiO_2$−5Cu can be caused by its dissolution in aluminum during mechanical alloying. The formation of a supersaturated solid solution of copper in aluminum as a result of mechanical alloying was noted in Ref. [33]. The formation of supersaturated solid solutions is the result of intense plastic deformation accompanying the process of mechanical alloying, which leads to a sharp increase in the density of crystalline defects and, as a consequence, acceleration of diffusion.

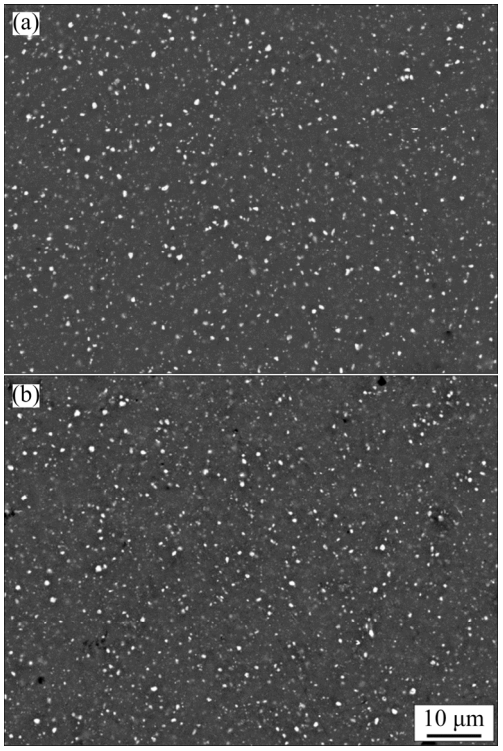


**Fig. 2** SEM images of Al−5$TiO_2$ powder particles with 2 wt.% PCA (a) and 5 wt.% Cu (b) after 10 h of milling

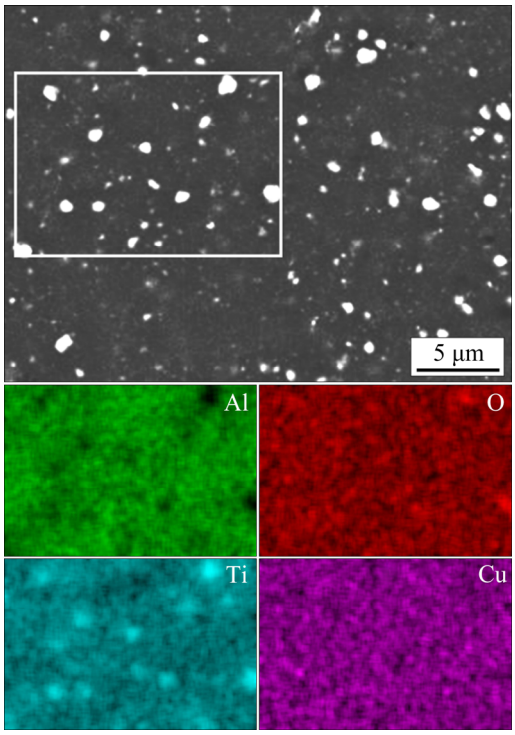


**Fig. 3** SEM image and elemental maps acquired from selected area for Al−5$TiO_2$−5Cu composite milled for 10 h

The obtained results indicate the completion of the mechanical alloying of aluminum with titanium oxide and the successful formation of granules of composite materials. Based on this, it can be concluded that the material with the PCA addition, due to its decomposition [34], in a short period of 8−10 h managed to go through the stages of welding and fracture, without which mechanical alloying would be impossible.

### 3.2 XRD analysis

The absence of reaction between aluminum and titanium oxides, as well as the effect of the dissolution of copper in aluminum is confirmed by X-ray phase analysis. So, Fig. 4 shows the XRD patterns of Al−5$TiO_2$ composite with the copper and PCA additions after 1 and 10 h of mechanical alloying. Figure 4(a) shows that the phase composition of the material with the PCA does not change during mechanical alloying: both after 1 h and 10 h, Al and $TiO_2$ diffraction lines are present in the XRD patterns. In the second material, after 1 h (Fig. 4(b)), in addition to the diffraction lines of these two phases, copper lines are present. However, after 10 h, there are no copper peaks. This is associated with its dissolution in aluminum and confirms the data of SEM and EDS analysis (see Fig. 3). Besides, in addition to the main phases of Al and $TiO_2$, a new phase line was detected in the diffraction pattern, which, according to the ICDD PDF−2 database, is likely to be a metastable phase of $Al_4Cu_9$. Its formation is unusual, since according to the data in Ref. [35], it is detected in the Al−Cu system only at a significantly higher copper content. This phase is formed in Cu-rich regions at short processing time until equilibrium $CuAl_2$ is precipitated, which is associated with low thermal activation.

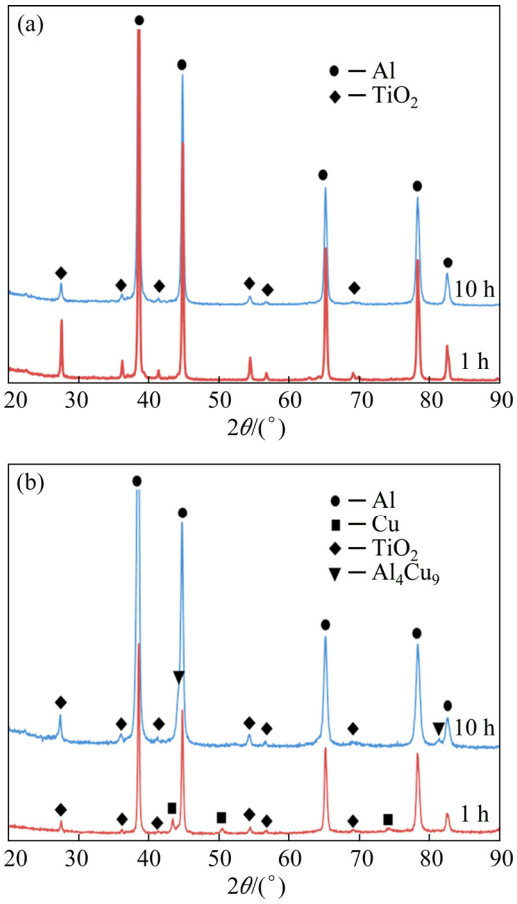


**Fig. 4** XRD patterns of Al−5$TiO_2$ powders with PCA (a) and Cu (b) additions after 1 and 10 h of milling

The dissolution of copper in aluminum is accompanied by a change in the lattice parameter of the aluminum solid solution, which affects the shift of Al diffraction peaks. Using the Nelson−Riley extrapolation function $1/2(\cos^2\theta/\sin\theta+\cos^2\theta/\theta)$ [36] the lattice parameter of the aluminum solid solution was determined in 1−10 h of treatment. The dependence of the calculated values on the duration of mechanical alloying is shown in Fig. 5(a). It

shows that with an increase in the processing time, the lattice parameter continuously decreases to 0.4043 nm, which is due to the fact that the atomic radius of copper is lower than that of aluminum. Thus, the process of mechanical alloying of aluminum with titanium oxide with 5 wt.% Cu is accompanied by two processes: the formation of a supersaturated solid solution of copper in aluminum and the formation of the $Al_4Cu_9$ phase.

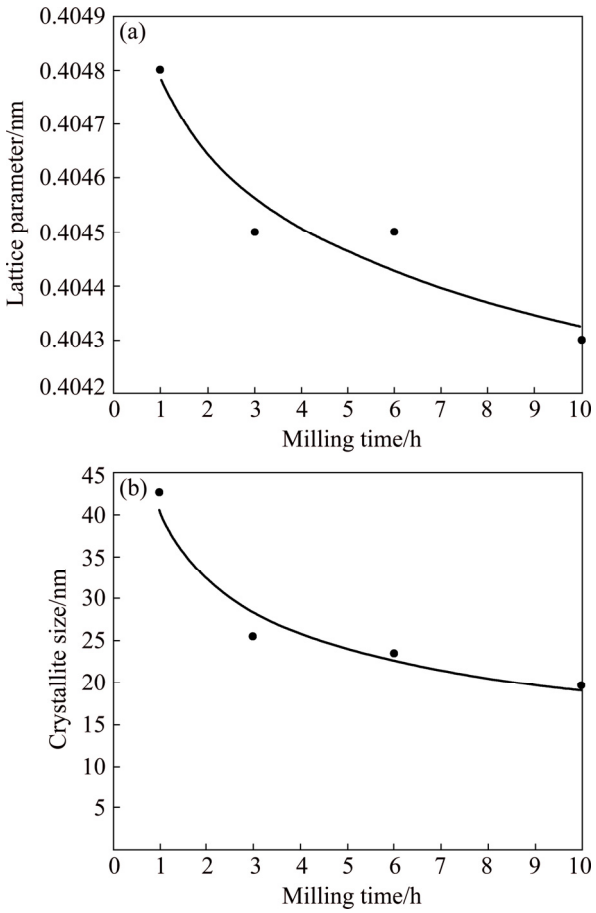


**Fig. 5** Effect of milling time on lattice parameter (a) and crystallite size (b) of aluminum solid solution for material with Cu addition

In addition to the shift of the aluminum lines in the diffraction patterns, their significant broadening was also revealed (Fig. 6). The broadening of Al diffraction lines was analyzed by the Williamson – Hall method [37], in which a graph drawn between $4\sin\theta$ and $\beta_{hkl}\cos\theta$ allows to determine the lattice strain and crystallite size from the slope of the straight line and the intersection with the vertical ordinate, respectively. This analysis showed that broadening is almost completely caused by a decrease in crystallite size ($D$), which is calculated as

$$D = \frac{K\lambda}{\beta\cos\theta} \quad (1)$$

where $K$ is a constant equal to 0.94 for spherical shaped particles, $\lambda$ is the X-ray wavelength (1.54056 Å) of incident radiation and $\beta$ is the instrumental corrected integral breadth of peak profile in radians.

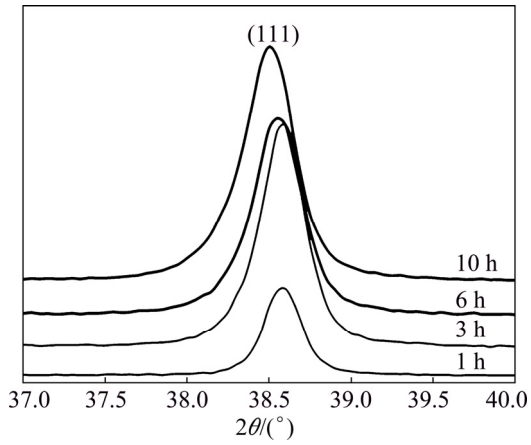


**Fig. 6** Diffraction peaks of Al (111) for Al−5$TiO_2$−5Cu material after different milling time

So, Fig. 5(b) shows the dependence of the size of aluminum crystallites calculated by this method with the Cu addition on the processing time. As can be seen from Fig. 5(b), the size of aluminum crystallites after 1 h of treatment is 43 nm. With a subsequent increase in processing to 10 h, the crystallite size gradually decreases to 20 nm.

The cause of nanocrystalline structure formation during mechanical alloying is as follows. The main deformation mechanism at high strain rates is formation of shear bands that consist of a dense network of dislocations. With continued milling, the average atomic level strain increases due to the increasing dislocation density, and at a certain dislocation density within these heavily strained regions, the crystal disintegrates into subgrains that are separated by low-angle grain boundaries [27]. This results in a decrease of the lattice strain. On further processing, deformation occurs in shear bands located in previously unstrained parts of the material. The grain size decreases steadily and the shear bands coalesce. The low-grain angle boundaries are replaced by the high-angle grain boundaries, implying grain rotation. Consequently, dislocation-free nanocrystalline grains are formed.

### 3.3 Microhardness evolution

The formation of a supersaturated solid solution and a decrease in grain size are some of the main reasons for the increase in the hardness of powder materials in the process of mechanical alloying [38]. Figure 7 shows the change in the microhardness of the powder particles of the studied materials during high-energy milling. It can be seen that with an increase in the processing time, the microhardness of the material with the Cu addition gradually increases to almost HV 290, reaching saturation by 10 h. The decay of the curve is associated with the complete dissolution of copper and the achievement of the steady-state stage of mechanical alloying [39]. In this stage, equilibrium is established between the welding and fracture of composite granules. At the same time, the composition of each granule corresponds to the composition of the initial powder mixture [27].

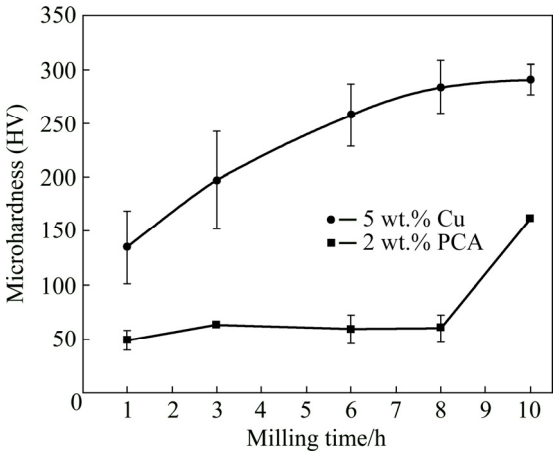


**Fig. 7** Effect of milling time on microhardness of Al−5$TiO_2$ with 5 wt.% Cu and 2 wt.% PCA additions

An increase in the microhardness of the material as a result of a decrease in grain size occurs by the mechanism of grain boundary hardening. It is well known that grain boundaries are effective barriers to migration of dislocations. The hardening effect depends on the deformation within one grain, locked at the grain boundary, where there are accumulations of dislocations depending on the grain size and stress concentration, which cause sliding in the neighboring grain. The smaller the grain size, the greater the number of these barriers on the path of sliding dislocations and the higher the stress required to maintain plastic deformation in the early stages [40]. The mechanism of solid solution hardening is that the dissolved atoms act as weak obstacles to the movement of dislocations, affecting their elastic energy [41]. In addition, during the mechanical alloying process, the distribution of harder titanium oxide particles in the metal matrix is improved. The more uniform the distribution of harder particles, the more efficient the load transfer mechanism. The load transfer from the soft matrix to the harder particles occurs through strain mismatch between the particles and matrix during straining due to the difference in their elastic modulus [42].

The opposite situation is observed in the case of the material with a PCA addition. Figure 7 shows that the microhardness of this material after a weak increase in the first 3 h of treatment practically does not change up to 8 h, and amounts to about HV 60. This behavior is consistent with the results of studying the morphology of powder particles (see Figs. 1(a, b)). During processing, aluminum particles undergo exclusively plastic deformation, and a small increase in hardness is mainly due to deformation hardening. However, with a further increase in milling time to 10 h, the microhardness sharply increases to HV 162. Such a rise is caused by the activation of mechanical alloying processes, which was suppressed as a result of the decomposition of the stearic acid, and, finally, the formation of granules of the Al−5$TiO_2$ composite (see Figs. 1(c) and 2(a)). Thus, the addition of copper contributes to the efficient mechanical alloying of aluminum with titanium oxide from an early milling time, and the addition of PCA, on the contrary, postpones this process.

### 3.4 Thermal transformation

The behavior of the studied materials during heating, up to melting and subsequent cooling, was studied using DSC analysis. DSC curves for powders milled for 10 h are shown in Fig. 8. In both cases, in the temperature range of 600−650 °C, the curves exhibit pronounced endothermic peak upon heating and exothermic peak upon cooling, which correspond to the melting and crystallization of aluminum respectively.

Two exothermic peaks appear on the curve for the material with a PCA addition (Fig. 8(a)) during heating at 700−850 °C, which are associated with the occurring of a reduction reaction between titanium oxide and aluminum [14], the equation of

which is as follows [17,25]:

$$13Al+3TiO_2 \rightarrow 3Al_3Ti+2Al_2O_3 \quad (2)$$

The first peak corresponds to the onset of the reaction, which is initiated at the Al/$TiO_2$ interface upon heating immediately after the melting of Al, which leads to the formation of the reaction product on the surface of $TiO_2$ particles. Further completion of the reaction is possible only by diffusion of the reagents through the product layer. Accordingly, the second exothermic peak on the DSC curve at a higher temperature indicates the completion of the reaction.

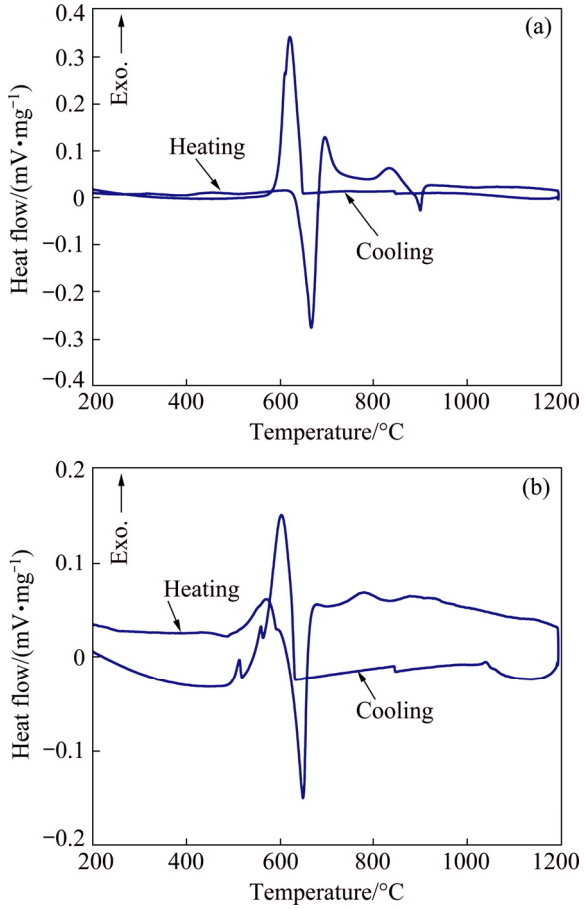


**Fig. 8** DSC curves of Al−5$TiO_2$ powders with 2 wt.% PCA (a) and 5 wt.% Cu (b) milled for 10 h

With a subsequent increase in temperature, an endothermic peak appears with a minimum at 900 °C, which is absent on the DSC curve of Al−5$TiO_2$ with copper addition (Fig. 8(b)). Its appearance is associated with carbon contamination of the powder resulting from the decomposition of stearic acid during milling or subsequent heating [43], which completely ends at about 550 °C for pure state [44]. Carbon is able to react with aluminum to form aluminum carbide, which was not detected by either XRD analysis in the as-milled condition or DSC. However, the presence of crystalline $Al_4C_3$ can be detected by XRD only after heating prior to the endothermic reaction [43,45]. A consequence of the presence of $Al_4C_3$ phase in the material is this endothermic peak, which corresponds to the chemical reaction of aluminum carbide with titanium aluminide formed earlier as a result of an exothermic reduction Reaction (2). Thus, the reaction corresponding to the endothermic peak is as follows:

$$3Al_3Ti+Al_4C_3 \rightarrow 3TiC+13Al \quad (3)$$

According to thermodynamic calculations performed in Ref. [45], the changes in enthalpy and Gibbs energy ($\Delta G$) are positive up to about 777 °C; above this temperature, $\Delta G$ becomes negative, which permits the reaction to proceed endothermically at higher temperatures. This is consistent with our results of DSC analysis. Besides, this endothermic effect may be attributed to melting of Al obtained from the reaction [46]. With a further increase in temperature up to 1200 °C and in the process of subsequent cooling, no thermal effects other than the corresponding aluminum crystallization are observed. Thus, the phase state of the material formed upon heating is final, and the resulting phases exhibit stability upon cooling. According to the intensity of X-ray lines in the XRD pattern shown in Fig. 9(a), it can be concluded that the material in the final state consists of the following main phases: Al, $Al_2O_3$ and TiC. The presence of weak lines of aluminum carbide and titanium aluminide on the X-ray diffraction pattern indicates incomplete Reaction (3). It should be noted that the formation of TiC as a result of the reaction between $Al_3Ti$ and $Al_4C_3$ in the Al−$TiO_2$−C system is possible only with an excess of Al and is not caused by a single reaction of $TiO_2$ with carbon [47].

In the case of copper addition, the main feature of the reduction reaction is that the first exothermic peak corresponding to its onset is observed on the DSC curve even before the aluminum melting (Fig. 8(b)). The second exothermic peak of low intensity, which is detected on the curve immediately after melting, is, apparently, a continuation of the first one. Thus, the chemical transformation begins in the solid state. The cause

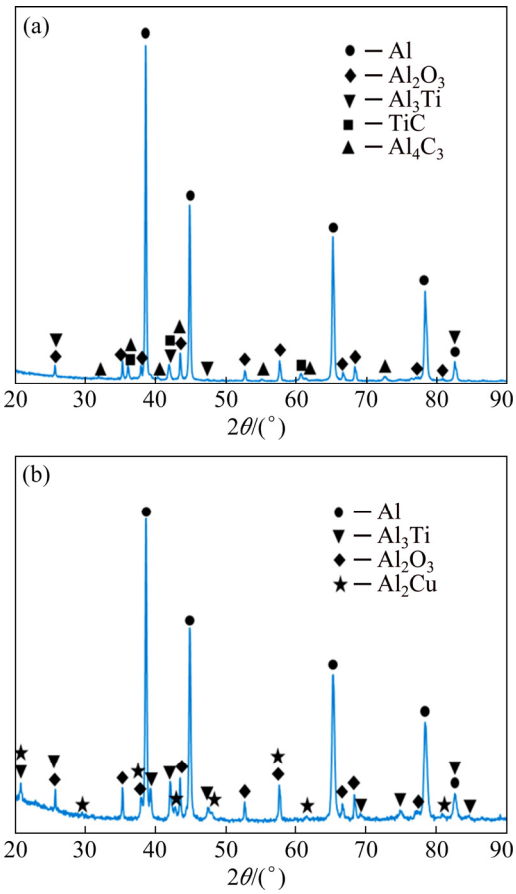


**Fig. 9** XRD patterns of Al−5$TiO_2$ powders with PCA (a) and Cu (b) additions milled for 10 h after heating to 1200 °C and subsequent cooling

of the decrease in the temperature of the onset of the exothermic reduction reaction is as follows. When the PCA is used in mechanical alloying, it or its decomposition products creates a thin film on the surface of aluminum and titanium oxide powder particles, which is a barrier that prevents direct contact between them for a chemical reaction [22]. When aluminum melts, this film disappears, and titanium oxide reacts with it. In the case of copper addition, such a barrier between the clean surfaces of aluminum and $TiO_2$ is absent; therefore, the reduction reaction begins at a lower temperature, even before the aluminum melts. The character of the DSC of the Al−5$TiO_2$ curve with the addition of copper is similar upon heating with the behavior of the Al−16.67wt.%$TiO_2$ material without PCA [16]. After the first exothermic peak, with an increase in temperature, two more peaks appear in the curve in the range of 700−950 °C, which is associated with a stepwise proceeding of the reduction reaction of residual titanium oxide.

In general, the reduction reaction during heating to 1200 °C is complete, as evidenced by the data of X-ray phase analysis presented in Fig. 9(b). So, as a result of all exothermic transformations, the final composition of the material is represented by the following main phases: Al, $Al_3Ti$ and $Al_2O_3$, which corresponds to Reaction (2) taking into account an excess of aluminum. The presence of the $Al_2Cu$ phase in the composition is associated with the appearance, on the DSC curve during cooling, of two small exothermic peaks, after the maximum exothermic peak corresponding to crystallization of aluminum. Their appearance should be caused by the precipitation of aluminum phase $Al_2Cu$ of eutectic origin.

### 3.5 Microstructure after laser melting

In order to evaluate the effect of laser melting process on the microstructure of investigated materials, single line tracks of mechanically alloyed powders were melted onto an aluminum substrate. The study results of the formed microstructure obtained using SEM are presented in Figs. 10 and 11. From Fig. 10(a) it is seen that the microstructure of the Al−5$TiO_2$ material with the PCA addition is heterogeneous. It contains white particles with size of about 1 μm randomly distributed in a dark gray aluminum matrix, which are the $Al_3Ti$ phase, according to EDS analysis (Fig. 10(b) and Table 1). Irregularly shaped regions of intermediate contrast should be $Al_2O_3$ particles. At a larger magnification in Al-rich areas, one can see darker dispersed particles indicated by arrows in Fig. 10(c). These particles are probably the $Al_4C_3$ phase, since its average atomic number is less than the atomic number of aluminum and, therefore, it has lower backscattered electron emission [48]. In the inset of this figure, aluminum grains are visible, at the boundaries of which there are a small number of particles of titanium aluminide. It should be noted that the determination of the true carbon content in the material, necessary for the detection of carbides, was hampered by the fact that the EDS analysis showed inadequately its high values in all areas. This is due to the fact that during electron bombardment, carbon, which is a product of the polymerization of hydrocarbons transmitted from the oil-rotary pump to the vacuum column, is deposited in the area under analysis [49]. However, according to the results of the analysis, it can be

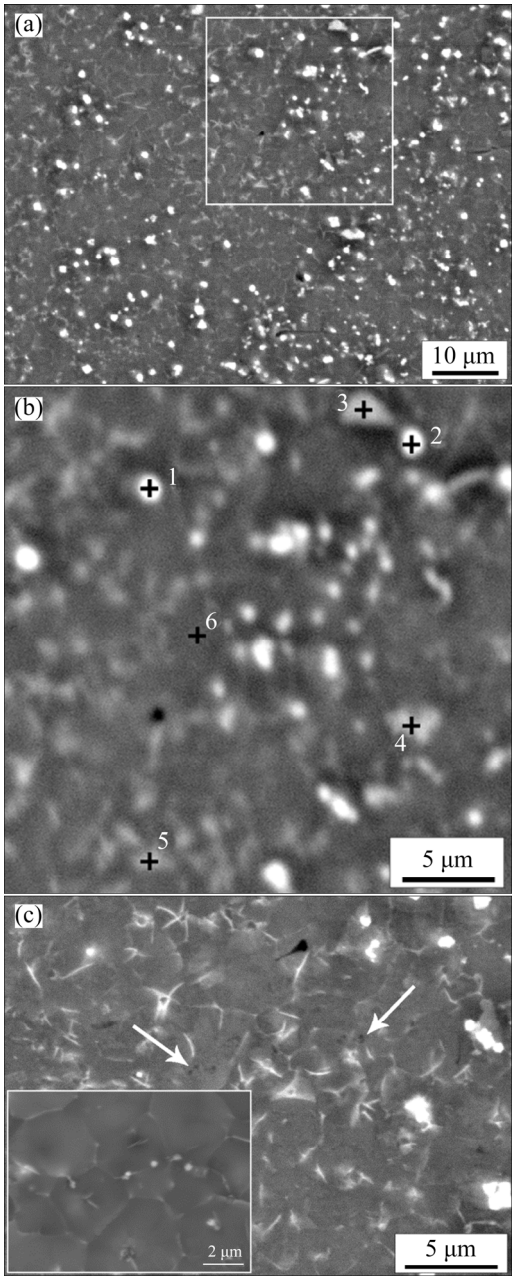


**Fig. 10** SEM image of laser melted powder of Al−$TiO_2$ with PCA addition (a), EDS analysis (b) of selected area in (a) and indicated regions, and magnified image (c)

**Table 1** Results of EDS elemental analysis results from Fig. 10(b)

| Spectrum label | Content/wt.% | | | |
|---|---|---|---|---|
| | Al | Ti | O | Total |
| 1 | 77.45 | 22.55 | − | 100.00 |
| 2 | 82.91 | 17.09 | − | 100.00 |
| 3 | 81.23 | 1.76 | 17.00 | 100.00 |
| 4 | 91.44 | 2.37 | 6.19 | 100.00 |
| 5 | 89.51 | 4.94 | 5.55 | 100.00 |
| 6 | 97.48 | 2.52 | 0.00 | 100.00 |

assumed that Reaction (3) does not have time to proceed during laser melting.

Figure 11(a) shows the microstructure of the copper-added material. As can be seen, the addition of copper leads to the formation of a homogeneous cellular structure after laser melting. According to EDS analysis (Fig. 11(b) and Table 2), the dark gray areas rich in aluminum are surrounded by a white layer rich in titanium or copper. From this we can conclude that the white structural component is a mixture of intermetallic phases: $Al_3Ti$ and $Al_2Cu$. The regions of intermediate contrast, as in the

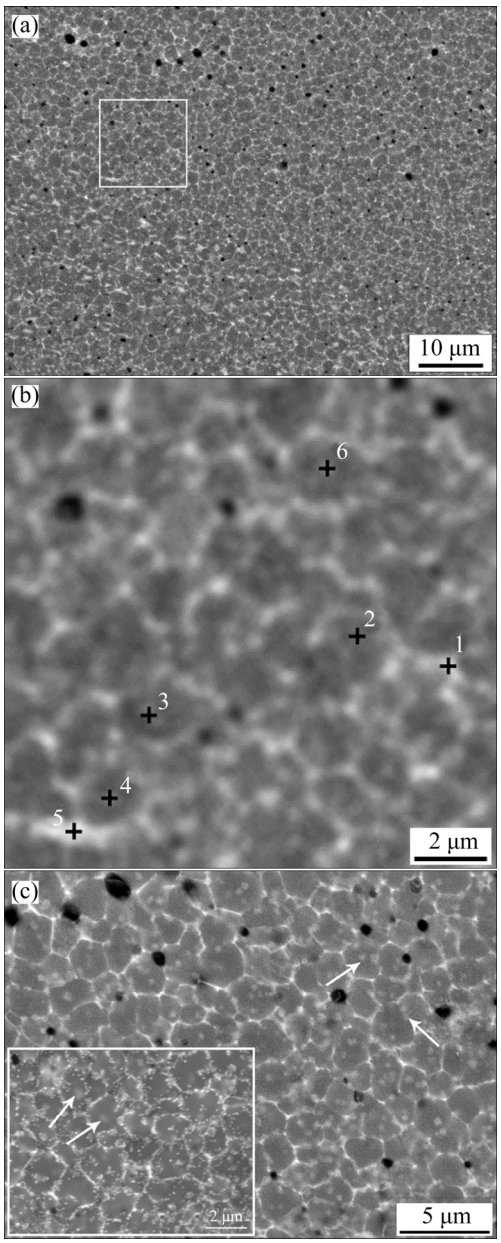


**Fig. 11** SEM image of laser melted powder of Al−$TiO_2$ material with Cu addition (a), EDS analysis of selected area in (a) and indicated regions (b) and magnified image (c)

**Table 2** EDS elemental analysis results from Fig. 11(b)

| Spectrum label | Content/wt.% | | | | |
|---|---|---|---|---|---|
| | Al | Ti | Cu | O | Total |
| 1 | 90.33 | 1.94 | 7.09 | 0.64 | 100.00 |
| 2 | 92.55 | 2.57 | 4.14 | 0.74 | 100.00 |
| 3 | 92.45 | 2.20 | 3.84 | 1.51 | 100.00 |
| 4 | 92.16 | 2.38 | 4.53 | 0.93 | 100.00 |
| 5 | 88.81 | 6.74 | 3.76 | 0.69 | 100.00 |
| 6 | 92.50 | 2.15 | 4.21 | 1.14 | 100.00 |

previous case, are aluminum oxide particles. These particles, clearly visible at a larger magnification (Fig. 11(c)), are found in the center of aluminum grains (shown by arrows). The size of both oxide particles and Al grains is much smaller than that in the material with the addition of PCA. It should be noted that rounded black regions are clearly visible in all the presented images. These are pores formed as a result of gas capture during melting [50]. On the inset of Fig. 11(c), disperse particles of aluminides evenly distributed along grain boundaries are also clearly distinguishable. Their size is about 100 nm. Such a structure should contribute to increased strength properties at elevated temperatures due to the pinning of aluminum grains by the particles. In addition, the fine-dispersed homogeneous structure of the material with the copper addition provides higher hardness at room temperature. So, despite the presence of porosity, the microhardness of laser-melted particles of Al−$TiO_2$ with Cu addition was higher than that of particles with PCA and reached HV (139±13) versus HV (72±12).

## 4 Conclusions

(1) Using Al−5$TiO_2$ as an example, it was shown that in the case when mechanical alloying of an aluminum-based material without PCA cannot be carried out, and its use is undesirable due to carbon contamination of the powder and subsequent formation of aluminum carbide, copper addition is a good solution for the successful formation of composite granules. So, the addition of 5 wt.% Cu promotes an efficient mechanical alloying of aluminum with titanium oxide from the beginning of milling, while the addition of PCA, on the contrary, postpones this process.

(2) After 10 h of milling, composite granules with a size of about 60 μm are formed, in which $TiO_2$ particles are uniformly distributed in the aluminum matrix. Moreover, the microhardness of the powder particles with the Cu addition amounts to HV 290, which is associated with its dissolution in aluminum.

(3) Subsequent heating of mechanically alloyed materials causes the activation of an exothermic reaction of titanium oxide reduction with aluminum, the start temperature of which, in the case of Cu addition, shifts to lower values, so that the transformation begins in the solid state.

(4) The Cu-added material after laser melting demonstrates a more dispersed and uniform structure compared to the material with the PCA addition, which positively affects its microhardness.

## Acknowledgments

The work was carried out with financial support from the Ministry of Education and Science of the Russian Federation in the framework of the State Assignment to the Universities (Project No.11.7172.2017/8.9). The Authors are grateful to V. V. Cheverikin and A. V. Pozdniakov for SEM studies.

## References

[1] OLAKANMI E O, COCHRANE R F, DALGARNO K W. A review on selective laser sintering/melting (SLS/SLM) of aluminium alloy powders: Processing, microstructure, and properties [J]. Progress in Materials Science, 2015, 74: 401−477.

[2] THOMPSON SCOTT M, BIAN L, SHAMSAEI N, YADOLLAHI A. An overview of direct laser deposition for additive manufacturing, Part I: Transport phenomena, modeling and diagnostics [J]. Additive Manufacturing, 2015, 8: 36−62.

[3] READ N, WANG W, ESSA K, ATTALLAH M M. Selective laser melting of AlSi10Mg alloy: Process optimization and mechanical properties development [J]. Materials & Design, 2015, 65: 417−424.

[4] MARCHESE G, AVERSA A, LORUSSO M, MANFREDI D, CALIGNANO F, LOMBARDI M, BIAMINO S, PAVESE M. Development and characterisation of aluminium matrix nanocomposites AlSi10Mg/$MgAl_2O_4$ by laser powder bed fusion [J]. Metals, 2018, 8(3): 175.

[5] SERCOMBE T B, LI X. Selective laser melting of aluminium and aluminium metal matrix composites: Review [J]. Materials Technology, 2016, 31: 77−85.

[6] ZHANG Hu, ZHU Hai-hong, QI Ting, HU Zhi-heng, ZENG Xiao-yan. Selective laser melting of high strength Al−Cu−Mg alloys: Processing, microstructure and

mechanical properties [J]. Materials Science and Engineering A, 2016, 656: 47−54.

[7] WANG P, DENG L, PRASHANTH K G, PAULY S, ECKERT J, SCUDINO S. Microstructure and mechanical properties of Al−Cu alloys fabricated by selective laser melting of powder mixtures [J]. Journal of Alloys and Compounds, 2018, 735: 2263−2266.

[8] AHUJA B, KARG M, NAGULIN K Y, SCHMIDT M. Fabrication and characterization of high strength Al−Cu alloys processed using laser beam melting in metal powder bed [J]. Physics Procedia, 2014, 56: 135−146.

[9] LI Neng, HUANG Shuai, ZHANG Guo-dong, QIN Ren-yao, LIU Wei, XIONG Hua-ping, SHI Gong-qi, BLACKBURN J. Progress in additive manufacturing on new materials [J]. Journal of Materials Science and Technology, 2019, 35: 242−269.

[10] ZHAO Xuan, GU Dong-dong, MA Cheng-long, XI Li-xia, ZHANG Han. Microstructure characteristics and its formation mechanism of selective laser melting SiC reinforced Al-based composites [J]. Vacuum, 2019, 160: 189−196.

[11] GU Dong-dong, WANG Zhi-yang, SHEN Yi-fu, LI Qin, LI Yu-fang. In-situ TiC particle reinforced Ti−Al matrix composites: Powder preparation by mechanical alloying and selective laser melting behavior [J]. Applied Surface Science, 2009, 255: 9230−9240.

[12] DANIEL B S S, MURTHY V S R, MURTY G S. Metal-ceramic composites via in-situ methods [J]. Journal of Materials Processing Technology, 1997, 68: 132−155.

[13] KIM J K, TJONG S C, MAI Yiu-Wing. Effect of interface strength on metal matrix composites properties [J]. Comprehensive Composite Materials II, 2018, 4: 22−59.

[14] DILIP J O S, REDDY B S B, DAS S, DAS K. In-situ Al-based bulk nanocomposites by solid-state aluminothermic reaction in Al−Ti−O system [J]. Journal of Alloys and Compounds, 2009, 475: 178−183.

[15] LIU Zhi-guang, RAYNOVA S, ZHANG De-liang, GABBITAS B. Study on the self sustained reactions in an Al−$TiO_2$ composite powder produced by high-energy mechanical milling [J]. Materials Science and Engineering A, 2007, 449−451: 1107−1110.

[16] FENG C F, FROYEN L. Formation of $Al_3Ti$ and $Al_2O_3$ from an Al−$TiO_2$ system for preparing in-situ aluminium matrix composites [J]. Composites: Part A, 2000, 31: 385−390.

[17] WELHAM N J. Mechanical activation of the formation of an alumina-titanium trialuminide composite [J]. Intermetallics, 1998, 6: 363−368.

[18] SHEN Y F, ZOU Z G, XIAO Z G, LIU K, LONG F, WU Y. Properties and electronic structures of titanium aluminides–alumina composites from in-situ SHS process [J]. Materials Science and Engineering A, 2011, 528: 2100−2105.

[19] ZHANG D L, YING D Y, MUNROE P. Formation of $Al_2O_3$ during heating of an Al/$TiO_2$ nanocomposite powder [J]. Journal of Materials Research, 2005, 20: 307−313.

[20] YING D Y, ZHANG D L, NEWBY M. Solid-state reactions during heating mechanically milled Al/$TiO_2$ composite powders [J]. Metallurgical and Materials Transactions A, 2004, 35: 2115−2125.

[21] LIU Z G, RAYNOVA S, ZHANG D L. Investigation of a discus-milling process using a powder mixture of Al and $TiO_2$ [J]. Metallurgical and Materials Transactions A, 2006, 37: 225−233.

[22] ALAMOLHODA S, HESHMATI-MANESH S, ATAIE A. Mechano-thermal treatment of $TiO_2$−Al powder mixture to prepare TiAl/$Al_2O_3$ composite [J]. Metals and Materials International, 2011, 17: 743−748.

[23] ALAMOLHODA S, HESHMATI-MANESH S, ATAIE A. Role of intensive milling in mechano-thermal processing of TiAl/$Al_2O_3$ nano-composite [J]. Advanced Powder Technology, 2012, 23: 343−348.

[24] CHEN Wei-ping, XIAO Hua-qiang, FU Zhi-qiang, FANG Si-cong, ZHU De-zhi. Reactive hot pressing and mechanical properties of $TiAl_3$/$Ti_3AlC_2$/$Al_2O_3$ in situ composite [J]. Materials & Design, 2013, 49: 929−934.

[25] WELHAM N J. Mechanical activation of the solid-state reaction between Al and $TiO_2$ [J]. Materials Science and Engineering A, 1998, 255: 81−89.

[26] SETOUDEH N, WELHAM N J. Effect of carbon on mechanically induced self-sustaining reactions (MSR) in $TiO_2$−Al−C mixtures [J]. International Journal of Refractory Metals and Hard Materials, 2016, 54: 210−215.

[27] SURYANARAYANA C. Mechanical alloying and milling [J]. Progress in Materials Science, 2001, 46: 1−184.

[28] LÜ L, LAI M O. Mechanical alloying [M]. Boston: Kluwer Academic Publishers, 1998.

[29] ZHANG Y F, LU L, YAP S M. Prediction of the amount of PCA for mechanical milling [J]. Journal of Materials Processing Technology, 1999, 89−90: 260−265.

[30] SHELEKHOV E V, SVIRIDOVA T A. Programs for X-ray analysis of polycrystals [J]. Metal Science and Heat Treatment, 2000, 42: 309−313.

[31] BENJAMIN J S, VOLIN T E. The mechanism of mechanical alloying [J]. Metallurgical Transactions, 1974, 5: 1929−1934.

[32] PROSVIRYAKOV A S, SHCHERBACHEV K D. Strengthening of mechanically alloyed Al-based alloy with high Zr contents [J]. Materials Science and Engineering A, 2018, 713: 174−179.

[33] FOGAGNOLO J B, AMADOR D, RUIZ-NAVAS E M, TORRALBA J M. Solid solution in Al−4.5wt%Cu produced by mechanical alloying [J]. Materials Science and Engineering A, 2006, 433: 45−49.

[34] KOLLO L, LEPAROUX M, BRADBURY C R, JÄGGI C, CARRENOMORELLI E, RODRÍGUEZ-ARBAIZAR M. Investigation of planetary milling for nano-silicon carbide reinforced aluminium metal matrix composites [J]. Journal of Alloys and Compounds, 2010, 489: 394−400.

[35] BESSON R, AVETTAND-FÈNOËL M N, THUINET L, KWON J, ADDAD A, ROUSSEL P, LEGRIS A. Mechanisms of formation of $Al_4Cu_9$ during mechanical alloying: An experimental study [J]. Acta Materialia, 2015, 87: 216−224.

[36] NELSON J B, RILEY D P. An experimental investigation of extrapolation methods in the derivation of accurate unit-cell dimensions of crystals [J]. Proceedings of the Physical Society, 1945, 57: 160−177.

[37] RAJENDER G, GIRI P K. Strain induced phase formation, microstructural evolution and bandgap narrowing in strained $TiO_2$ nanocrystals grown by ball milling [J]. Journal of

Alloys and Compounds, 2016, 676: 591−600.
[38] PROSVIRYAKOV A S, SHCHERBACHEV K D, TABACHKOVA N Y. Microstructural characterization of mechanically alloyed Al−Cu−Mn alloy with zirconium [J]. Materials Science and Engineering A, 2015, 623: 109−113.
[39] PROSVIRYAKOV A S, SHCHERBACHEV K D, TABACHKOVA N Y. Investigation of nanostructured Al−10wt.%Zr material prepared by ball milling for high temperature applications [J]. Materials Characterization, 2017, 123: 173−177.
[40] MORRIS D G. The origins of strengthening in nanostructured metals and alloys [J]. Revista de Metalurgia, 2010, 46: 173−186.
[41] MA Bing-yang, SHI Kai-cheng, SHANG Hai-long, LI Rong-bin, LI Ge-yang. The solid solution strengthening in Al−Zr nanocrystalline alloy films [J]. Surface and Coatings Technology, 2017, 321: 52−56.
[42] PROSVIRYAKOV A, BAZLOV A, POZDNIAKOV A, EMELINA N. Low-cost mechanically alloyed copper-based composite reinforced with silicate glass particles for thermal applications [J]. JOM, 2019, 71: 995−1001.
[43] KLEINER S, BERTOCCO F, KHALID F A, BEFFORT O. Decomposition of process control agent during mechanical milling and its influence on displacement reactions in the Al−$TiO_2$ system [J]. Materials Chemistry and Physics, 2005, 89: 362−366.
[44] JAW K S, HSU C K, LEE J S. The thermal decomposition behaviors of stearic acid, paraffin wax and polyvinyl butyral [J]. Thermochimica Acta, 2001, 367−368: 165−168.
[45] NUKAMI T, FLEMINGS M C. In situ synthesis of TiC particulate-reinforced aluminum matrix composites [J]. Metallurgical and Materials Transactions, 1995, 26: 1877−1884.
[46] MEHRIZI M Z, MOSTAAN H, BEYGI R, RAFIEI M, ABBASIAN A R. Reaction pathways of nanocomposite synthesized in-situ from mechanical activated Al−C−$TiO_2$ powder mixture [J]. Russian Journal of Non-Ferrous Metals, 2018, 59: 117−122.
[47] KIM Je-Woo, LEE Jung-Moo, LEE Joon-Ho, LEE Jae-Chul. Role of excess Al on the combustion reaction in the Al−$TiO_2$−C system [J]. Metals and Materials International, 2014, 20: 1151−1156.
[48] LLOYD G E. Atomic number and crystallographic contrast images with the SEM: A review of backscattered electron techniques [J]. Mineralogical Magazine, 1987, 51: 3−19.
[49] WASSILKOWSKA A, CZAPLICKA-KOTAS A, ZIELINA M, BIELSKI A. An analysis of the elemental composition of micro-samples using EDS technique [J]. Technical Transactions, 2014, 1: 133−148.
[50] ZHANG Jin-liang, SONG Bo, WEI Qing-song, BOURELL D, SHI Yu-sheng. A review of selective laser melting of aluminum alloys: Processing, microstructure, property and developing trends [J]. Journal of Materials Science & Technology, 2019, 35: 270−284.

# 添加 Cu 对机械合金化 Al−Ti−O 原位复合材料显微组织演变和硬化的影响

A. S. PROSVIRYAKOV, A. I. BAZLOV, I. S. LOGINOVA

Department of Physical Metallurgy of Non-Ferrous Metals,
National University of Science and Technology “MISiS”, Leninskiy Prospect 4, Moscow 119049, Russia

**摘　要：**研究添加 5% Cu 和 2%(质量分数)硬脂酸(工艺控制剂，PCA)的 Al−5%$TiO_2$(质量分数)复合材料在机械合金化和后续加热过程中显微组织的形成和强化。采用高能球磨法制备粉末复合材料，球磨时间长达 10 h。用激光熔融对单线轨的粉末进行处理。利用光学和扫描电镜、X 射线衍射分析技术和差示扫描量热法研究其显微组织演变。结果表明，Cu 的加入能促进铝与 $TiO_2$ 在球磨过程中的有效机械合金化，使粉末具有更高的显微硬度(高达 HV 290)；而 PCA 的效果恰恰相反。在这两种情况下，都形成了均匀分布的 $TiO_2$ 复合颗粒。机械合金化材料的后续加热导致 $TiO_2$ 与铝的放热反应，使得含 Cu 材料的开始反应温度变得更低，从固态开始发生转变。此外，激光熔融后含 Cu 材料具有更加分散和均匀的结构，有利于提高其显微硬度。

**关键词：**机械合金化；Al−Ti−O 系；铝基复合材料；显微组织；硬化；激光熔融

**(Edited by Xiang-qun LI)**